chemistry

MDPI

Article

Synthesis and Antidiabetic Evaluation of Triazole-Linked Thiazolidine-2,4-dione Hybrids as α-Glucosidase and α-Amylase Inhibitors

Subhayan Das Pal [1,2], Yukta Sao [1,2], Sujeet Kumar [3], Nishith Teraiya [4], Basavaraj Metikurki [3], Shankar G. Alegaon [2,5], Sanjana S. Prakash [2,6], Gururaj Kudur Jayaprakash [7,*] and Subhas S. Karki [1,2,*]

1 Department of Pharmaceutical Chemistry, KLE College of Pharmacy (KLE Deemed to be University), Bengaluru 560010, India; subhayan1701@gmail.com (S.D.P.); yukta2603@gmail.com (Y.S.)
2 Department of Pharmaceutical Chemistry, KLE Academy of Higher Education and Research (KLE Deemed to be University), Belagavi 590010, India; sgalegaon@gmail.com (S.G.A.); sanjanasp307@gmail.com (S.S.P.)
3 Department of Pharmaceutical Chemistry, Nitte College of Pharmaceutical Sciences (Nitte Deemed to be University), Yelahanka, Bengaluru 560064, India; dr.sujeethkumar@nitte.edu.in (S.K.); basavrajumetikurki@nitte.edu.in (B.M.)
4 Department of Pharmaceutical Chemistry, K.B Institute of Pharmaceutical Education and Research, Kadi Sarva Vishvavidyalaya, Gandhinagar 382023, India; teraiya@gmail.com
5 Department of Pharmaceutical Chemistry, KLE College of Pharmacy (KLE Deemed to be University), Belagavi 590010, India
6 Department of Pharmaceutics, KLE College of Pharmacy (KLE Deemed to be University), Bengaluru 560010, India
7 Department of Chemistry, Nitte Meenakshi Institute of Technology (Nitte Deemed to be University), Yelahanka, Bengaluru 560064, India
* Correspondence: rajguru97@gmail.com (G.K.J.); subhashskarki@klepharmblr.org or subhasskarki@gmail.com (S.S.K.)

Abstract

A series of 1,2,3-triazole-linked-thiazolidine-2,4-dione hybrids (**SDP1–SDP15**) were designed, synthesized, and evaluated for their antidiabetic potential. All structures were characterized by FT-IR and NMR spectroscopy (^{1}H and ^{13}C). All derivatives exhibited significant in vitro inhibition of α-glucosidase (IC_{50}: 24.17–46.41 µg/mL) and α-amylase (23.25–50.66 µg/mL), comparable to the standard drug acarbose (IC_{50}: 25.18 and 32.53 µg/mL) and superior to the reference drug pioglitazone (IC_{50}: 84.24 and 79.74 µg/mL) for α-glucosidase and α-amylase, respectively. Molecule **SDP8** emerged as the most potent with an IC50 of 24.17 and 23.25 µg/mL for α-glucosidase and α-amylase, respectively. Further, **SDP8** exhibited a higher docking score of −10.7 kcal/mol and −10.4 kcal/mol against α-glucosidase and α-amylase than pioglitazone (−8.1 kcal/mol and −7.7 kcal/mol, respectively), suggesting that interaction with these two enzymes may be the cause for its antidiabetic activity. Furthermore, DFT analysis revealed favorable electronic properties with a low HOMO-LUMO energy gap, whereas ADMET predictions revealed moderate drug-like characteristics with some limitations, such as poor solubility, relatively high lipophilicity, and partial noncompliance with drug-likeness regulations. Overall, these results highlight triazole-linked thiazolidinedione hybrids as promising candidates for further development in T2DM, with **SDP8** serving as a preliminary lead requiring additional optimization and validation.

Keywords: type 2 diabetes mellitus; thiazolidinedione-triazole hybrids; α-amylase; α-glucosidase

Check for updates

Academic Editors: Carmen Di Giovanni and Antonio Lavecchia

Received: 21 April 2026
Revised: 26 May 2026
Accepted: 27 May 2026
Published: 4 June 2026

Copyright: © 2026 by the authors. Licensee MDPI, Basel, Switzerland. This article is an open access article distributed under the terms and conditions of the Creative Commons Attribution (CC BY) license.

1. Introduction

Type 2 diabetes mellitus (T2DM) is characterized by persistent hyperglycemia resulting from impaired insulin secretion. It accounts for approximately 90–95% of all diabetic cases [1]. The global burden of T2DM has increased significantly recently. Approximately 589 million diabetic cases were reported globally in 2024, which is projected to reach 643 million by 2030 [2,3]. These alarming figures highlight the inadequacy of current antidiabetic drugs, emphasizing the urgent need for an effective molecule targeting multiple pathways in T2DM.

The key therapeutic targets involved in carbohydrate digestion and glucose homeostasis in T2DM are α-glucosidase and α-amylase; α-amylase initiates the hydrolysis of complex polysaccharides into oligosaccharides, while α-glucosidase further catalyzes their breakdown into absorbable monosaccharides, such as glucose [4,5]. Inhibition of these enzymes delays carbohydrate digestion and glucose absorption in the intestine, thereby reducing postprandial hyperglycemia, a major contributor to the progression of type 2 diabetes [6]. According to Leszek's review study, certain neurodegenerative disorders such as Alzheimer's disease, Parkinson's disease, Huntington's disease, and amyotrophic lateral sclerosis are linked to diabetes mellitus, particularly type 2 diabetes [7]. A serious, long-term microvascular consequence that develops in the later stages of diabetes is diabetic nephropathy (DN). The complicated pathophysiology of DN causes a number of anomalies in kidney structure, including altered renal hemodynamics, aberrant glucose and lipid metabolism, polyol pathway dysfunction, oxidative stress, and inflammatory reactions. The preventive effect of lycorine hydrochloride against diabetic nephropathy has been described by Fang and colleagues [8].

Additionally, modulation of these enzymes helps in controlling rapid glucose fluctuations and improves overall glycemic control. Therefore, targeting α-glucosidase and α-amylase represents an effective strategy for the management of T2DM [9,10].

Thiazolidine-2,4-dione (TZD) derivatives have also been explored for their potential as inhibitors of carbohydrate-hydrolyzing enzymes such as α-glucosidase and α-amylase, offering an alternative mechanism for antidiabetic activity. Several studies have reported that structural modification of the TZD scaffold can yield compounds with significant inhibitory activity against these enzymes, thereby reducing postprandial hyperglycemia. For instance, modified TZD derivatives bearing benzylidene or heterocyclic substitutions have demonstrated potent α-glucosidase inhibition with improved selectivity and reduced side effects compared to standard drugs [11,12]. Similarly, other reports have highlighted TZD-based hybrids exhibiting dual α-glucosidase and α-amylase inhibitory activity, suggesting their role in delaying carbohydrate digestion and glucose absorption [13,14]. These findings indicate that TZD derivatives remain a promising scaffold for the development of safer and more effective inhibitors targeting α-glucosidase and α-amylase [15,16].

In parallel, triazole-based derivatives have also emerged as potent pharmacophores in antidiabetic drug discovery. The incorporation of 1,2,3-triazole moieties has been shown to improve metabolic stability, bioavailability, and receptor binding affinity of the designed molecule. For instance, Kumar et al. have reported a series of 1,2,3-triazole-linked hybrids exhibiting significant α-glucosidase inhibitory activity with improved pharmacokinetic profiles, highlighting their potential as antidiabetic agents [17]. Similarly, Patel et al. have reported triazole derivatives demonstrating dual inhibition of α-amylase and α-glycosidase [18–20]. Consequently, the integration of thiazolidine-2,4-dione (TZDs) with 1,2,3-triazole moieties represents a promising lead for the development of potential enzyme inhibitors (Figure 1).

In the present study, we report on the synthesis and invitro enzyme inhibitory property of novel 1,2,3-triazole-linked thiazolidine-2,4-dione hybrids, followed by in silico investiga-

tion to elucidate binding interactions and mechanistic insights. This integrated approach aims to develop promising antidiabetic agents with selectivity against both the enzymes.

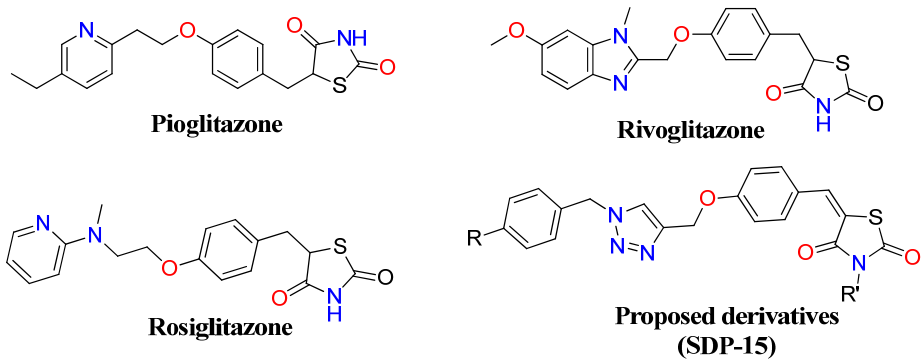

Figure 1. Clinically used thiazolidine-2,4-diones.

2. Materials and Methods

2.1. Chemicals and Reagents

All reagents and solvents were purchased from BLD Pharma, Hyderabad, and Spectrochem Pvt. Ltd., Bengaluru, India. Progress of the reaction was monitored on pre-coated silica gel plates 60 F254 from Merck India Ltd. (Darmstadt, Germany). The melting point of all synthesized molecules was established with a digital melting point apparatus (DBK 50 Hz, 220 V) and reported uncorrected. The proton nuclear magnetic resonance (^{1}Hand ^{13}C NMR) spectra were recorded at 400 MHz on a Bruker (Billerica, MA, USA), Avance-III NMR spectrometer in deuterated chloroform ($CDCl_3$) and dimethyl sulfoxide (DMSO-$_{d6}$). The Fourier transform infrared (FTIR) spectra were obtained on a JASCO 460+, Tokyo, Japan. The HRMS were taken on Waters (Milford, MA, USA) Xevo G2 QTOF and ACQUITY UPLC (Waters, Milford, MA, USA). *N*-substituted thiazolidindiones (**3a–c**) were obtained by reacting thiazolidin-2,4-dione (**1**) and appropriate phenacyl bromides (**2a–c**), as per the literature [21]. Then, 4-(prop-2-ynyloxy)benzaldehyde was prepared by reacting 4-hydroxybenzaldehyde (**4**) and propargyl bromide (**5**) [22]. The different arylazides (**9a–e**) were obtained by reacting p-substituted benzyl chlorides (**7a–e**) and sodium azide (**8**) in a mixture of acetone and water, as per the procedure reported earlier [23]. Then, 4-((1-Benzyl-1*H*-1,2,3-triazol-4-yl)methoxy)benzaldehydes (**10a–e**) were obtained by a reaction between 4-(prop-2-ynyloxy)benzaldehyde (**6**) and different *p*-substituted benzyl azides (**9a–e**), as per the literature [24].

*2.2. General Procedure for Synthesis of P-Substituted-3-benzoyl-5-(4-((1-benzyl-1H-1,2,3-triazol-4-Yl)methoxy)benzylidene)thiazolidine-2,4-dione (***SDP1–SDP15***)*

An equimolar quantity (1 mM) of *p*-substituted-3-benzoylthiazolidine-2,4-dione (**3a–c**) and 4-((1-benzyl-1*H*-1,2,3-triazol-4-yl)methoxy)benzaldehydes (**10a–e**) was refluxed for 2 h in 25 mL of methanol and 2 drops of piperidine. The precipitated mass was filtered and recrystallized from the DMF and ethanol mixture.

Code	R	R′	Code	R	R′	Code	R	R′
SDP1	$-NO_2$	H	**SDP6**	$-NO_2$	$-CH_3$	**SDP11**	$-NO_2$	-Br
SDP2	H	H	**SDP7**	H	$-CH_3$	**SDP12**	H	-Br
SDP3	$-CH_3$	H	**SDP8**	$-CH_3$	$-CH_3$	**SDP13**	$-CH_3$	-Br
SDP4	$-OCH_3$	H	**SDP9**	$-OCH_3$	$-CH_3$	**SDP14**	$-OCH_3$	-Br
SDP5	-Cl	H	**SDP10**	-Cl	$-CH_3$	**SDP15**	-Cl	-Br

2.2.1. 5-(4-((1-(4-Nitrobenzyl)-1*H*-1,2,3-triazol-4-Yl)methoxy)benzylidene)-3-(2-oxo-2-phenylethyl)thiazolidine-2,4-dione (**SDP1**)

White amorphous powder, m.p: 230–232 °C, yield: 66, R_f: 0.64: IR (KBr, ν_{max}, cm^{-1}): 3157–3015 (C-H, ar.), 2938–2874 (C-H), 1677 (C=O), 1504 (C=C); ^{1}H NMR ($CDCl_3$; 400 MHz) δ ppm: 5.20 (s, 2H, -CH_2-), 5.29 (s, 2H, -CH_2-), 5.55 (s, 2H, -CH_2-), 7.12 (d, 2H, *J* = 8.8 Hz), 7.26 (d, 2H, *J* = 8.4 Hz), 7.40 (d, 2H, *J* = 8.4 Hz), 7.51–7.58 (m, 5H), 7.67 (t, 1H, *J* = 16 Hz), 7.92 (s, 1H), 8.03 (d, 2H, *J* = 7.2 Hz). ^{13}C-NMR (DMSO-d_6, 400 MHz) δ ppm: 47.42, 53.59, 62.14, 115.59, 118.79, 122.70, 126.44, 128.17, 128.96, 129.44, 129.48, 132.32, 132.84, 134.13, 134.20, 134.28, 144.05, 153.04, 160.05, 166.06, 189.82. M.F: $C_{28}H_{21}N_5O_6S$. HRMS *m*/*z* (ES+): $[M + H]^+$ 556.1213 (556.1354). Purity %: 99.89.

2.2.2. 5-(4-((1-Benzyl-1*H*-1,2,3-triazol-4-Yl)methoxy)benzylidene)-3-(2-oxo-2-phenylethyl)thiazolidine-2,4-dione (**SDP2**)

White amorphous powder, m.p: 190–192 °C, yield: 66, R_f: 0.59: IR (KBr, ν_{max}, cm^{-1}): 3140–3033 (C-H), 2938–2724 (C-H), 1676 (C=O), 1508 (C=C); ^{1}H-NMR(DMSO-d_6; 400 MHz) δ ppm: 5.26 (s, 2H, -CH_2-), 5.33 (s, 2H, -CH_2-), 5.63 (s, 2H, -CH_2-), 7.26 (d, 2H, *J* = 8 Hz), 7.32–7.39 (m, 5H), 7.60–7.67 (td, 4H, *J* = 16, 8 Hz), 7.76 (t, 1H, *J* = 16 Hz), 7.98 (d, 1H, *J* = 8 Hz), 8.11 (d, 2H, *J* = 8 Hz), 8.33 (s, 1H). ^{13}C-NMR (DMSO-d_6, 400 MHz)-δ ppm: 48.36, 52.44, 61.82, 116.26, 118.23, 124.42, 125.82, 126.12, 128.78, 129.55, 132.89, 134.28, 143.12, 143.83, 160.55, 165.81 M.F: $C_{28}H_{22}N_4O_4S$. HRMS *m*/*z* (ES+): $[M + H]^+$ 511.1362 (511.1394). Purity %: 99.98.

2.2.3. 5-(4-((1-(4-Methylbenzyl)-1*H*-1,2,3-triazol-4-Yl)methoxy)benzylidene)-3-(2-oxo-2-phenylethyl)thiazolidine-2,4-dione (**SDP3**)

White crystalline powder, m.p: 201–203 °C, yield: 71, R_f: 0.58: IR (KBr, ν_{max}, cm^{-1}): 3161–3013 (C-H), 2937–2875 (C-H), 1677 (C=O), 1513 (C=C); ^{1}H-NMR ($CDCl_3$; 400 MHz) δ ppm: 2.39 (s, 3H, -CH_3), 5.20 (s, 2H, -CH_2-), 5.26 (s, 2H, -CH_2-), 5.53 (s, 2H, -CH_2-), 7.12 (d, 2H, *J* = 8.4 Hz), 7.21 (s, 4H), 7.50–7.57 (dt, 5H, *J* = 7.6, 16.4 Hz), 7.67 (t, 1H, *J* = 15.2 Hz), 7.92 (s, 1H), 8.01 (d, 2H, *J* = 8.0 Hz). ^{13}C-NMR (DMSO-d_6, 400 MHz) δ ppm: 21.18, 47.41, 54.16, 115.61, 118.70, 126.66, 126.35, 128.17,128.23, 128.96, 129.86, 131.30, 132.31, 134.19, 134.29, 139.18, 143.73, 160.14, 166.07, 189.83. M.F: $C_{29}H_{24}N_4O_4S$. HRMS *m*/*z* (ES+): $[M + H]^+$ 525.1518 (525.1540). Purity %: 99.96.

2.2.4. 5-(4-((1-(4-Methoxybenzyl)-1*H*-1,2,3-triazol-4-Yl)methoxy)benzylidene)-3-(2-oxo-2-phenylethyl)thiazolidine-2,4-dione (**SDP4**)

White amorphous powder, m.p: 197–199 °C, yield: 68, R_f: 0.61: IR (KBr, ν_{max}, cm^{-1}): 3163–3014 (C-H), 2937–2842 (C-H), 1692 (C=O), 1513 (C=C); ^{1}H-NMR ($CDCl_3$; 400 MHz) δ ppm: 3.84 (s, 3H, OCH_3), 5.20 (s, 2H, -CH_2-), 5.26 (s, 2H, -CH_2-), 5.50 (s, 2H, -CH_2-), 6.94 (d, 2H, *J* = 8.0 Hz), 7.12 (d, 2H, *J* = 8.0 Hz), 7.26 (s, 2H), 7.50–7.57 (m, 5H), 7.67 (t, 1H, *J* = 14.8 Hz), 7.92 (s, 1H), 8.03 (d, 2H, *J* = 8.0 Hz). ^{13}C-NMR (DMSO-d_6, 400 MHz) δ ppm: 47.41, 53.90, 55.37, 62.20, 114.56, 115.61, 122.53, 126.27, 126.36, 128.17, 128.96, 129.78, 143.94. M.F: $C_{29}H_{24}N_4O_5S$. HRMS *m*/*z* (ES+): $[M + H]^+$ 541.1467 (541.1518). Purity %: 99.98.

2.2.5. 5-(4-((1-(4-Chlorophenyl)-1*H*-1,2,3-triazol-4-Yl)methoxy)benzylidene)-3-(2-oxo-2-phenylethyl)thiazolidine-2,4-dione (**SDP5**)

White amorphous powder, m.p: 185–187 °C, yield: 68, R_f: 0.61: IR (KBr, ν_{max}, cm^{-1}): 3160–3013 (C-H), 2975–2875 (C-H), 1677 (C=O), 1513 (C=C); ^{1}H-NMR ($CDCl_3$; 400 MHz) δ ppm. 5.20 (s, 2H, –CH_2–), 5.28 (s, 2H, –CH_2–), 5.58 (s, 2H, –CH_2–), 7.12 (d, 2H, *J* = 8.8 Hz), 7.29–7.32 (m, 2H), 7.40–7.42 (m, 3H), 7.50–7.57 (td, 4H, *J* = 15.6, 8.4 Hz), 7.67 (t, 2H, *J* = 14.8 Hz), 7.91 (s, 1H), 8.03 (d, 2H, *J* = 8 Hz). ^{13}C-NMR (DMSO-d_6, 400 MHz)-δ ppm: 47.41, 54.34, 62.18, 115.61, 118.71, 122.78, 126.37, 128.17, 128.92, 128.95, 129.21, 132.31, 134.17,

134.28, 134.35, 143.82, 160.12, 166.06, 167.82, 189.84. M.F: $C_{28}H_{21}ClN_4O_4S$. HRMS *m*/*z* (ES+): $[M + H]^+$ 545.0972 (545.0944). Purity %: 94.24.

2.2.6. 5-(4-((1-(4-Nitrobenzyl)-1*H*-1,2,3-triazol-4-Yl)methoxy)benzylidene)-3-(2-oxo-2-(P-tolyl)ethyl)thiazolidine-2,4-dione (**SDP6**)

White amorphous powder, m.p: 212–214 °C, yield: 72, R_f: 0.64: IR (KBr, ν_{max}, cm^{-1}): 3159–3014 (C-H), 2978–2870 (C-H), 1676 (C=O), 1511 (C=C); ^{1}H NMR ($CDCl_3$; 400 MHz) δ ppm: 2.47 (s, 3H, -CH_3), 5.17 (s, 2H, -CH_2-), 5.28 (s, 2H, -CH_2-), 5.54 (s, 2H, -CH_2-), 7.11 (d, 2H, *J* = 8.8 Hz), 7.26 (d, 2H, *J* = 8.4 Hz), 7.35 (d, 2H, *J* = 8.0 Hz), 7.40 (d, 2H, *J* = 8.4 Hz), 7.52 (d, 2H, *J* = 8.8 Hz), 7.58 (s, 1H), 7.92–7.90 (m, 3H).^{13}C-NMR (DMSO-d_6, 400 MHz) δ ppm:21.80, 53.59, 55.84, 62.15, 115.59, 115.69, 122.68, 126.48, 128.26, 129.43, 129.46, 129.61, 131.83, 132.18, 132.28, 134.02, 143.73, 145.21, 160.03, 166.09, 167.80, 189.36. M.F: $C_{29}H_{23}N_5O_6S$. HRMS *m*/*z* (ES+): $[M + H]^+$ 570.1369 (570.1559). Purity %: 99.53.

2.2.7. 5-(4-((1-Benzyl-1*H*-1,2,3-triazol-4-Yl)methoxy)benzylidene)-3-(2-oxo-2-(P-tolyl)ethyl)thiazolidine-2,4-dione (**SDP7**)

White crystalline powder, m.p: 218–220 °C, yield: 76, R_f: 0.56: IR (KBr, ν_{max}, cm^{-1}): 3154–3034 (C-H), 2936–2868 (C-H), 1676 (C=O), 1511 (C=C); ^{1}H-NMR ($CDCl_3$; 400 MHz) δ ppm: 2.47 (s, 3H, -CH_2-), 5.18 (s, 2H, -CH_2-), 5.31 (s, 2H, -CH_2-), 5.72 (s, 2H, -CH_2-), 7.13 (d, 2H, *J* = 8.0 Hz), 7.35 (d, 2H, *J* = 8.4 Hz), 7.46 (d, 2H, *J* = 8.4 Hz), 7.53 (d, 2H, *J* = 6.8 Hz), 7.91 (t, 4H, *J* = 8.0 Hz), 8.28 (d, 2H, *J* = 8.4 Hz). ^{13}C-NMR (DMSO-d_6, 400 MHz) δ ppm: 21.81, 47.34, 53.15, 62.08, 115.56, 124.40, 128.26, 128.66, 129.62, 132.30, 133.93, 166.27, 189.43. M.F: $C_{29}H_{24}N_4O_4S$. HRMS *m*/*z* (ES+): $[M + H]^+$ 525.1518 (525.1542). Purity %: 99.96.

2.2.8. 5-(4-((1-(4-Methylbenzyl)-1*H*-1,2,3-triazol-4-Yl)methoxy)benzylidene)-3-(2-oxo-2-(P-tolyl)ethyl)thiazolidine-2,4-dione (**SDP8**)

White crystalline powder, m.p: 222–224 °C, yield: 73, R_f: 0.58: IR (KBr, ν_{max}, cm^{-1}): 3158–3032 (C-H), 2975–2870 (C-H), 1677 (C=O), 1511 (C=C); ^{1}H NMR ($CDCl_3$; 400 MHz) δ ppm: 2.38 (s, 3H, -CH_3), 2.47 (s, 3H, -CH_3), 5.17 (s, 2H, -CH_2-), 5.23 (s, 2H, -CH_2-), 5.26 (s, 2H, -CH_2-), 7.11 (d, 2H, *J* = 8.4 Hz), 7.21 (s, 4H), 7.35 (d, 2H, *J* = 8.0 Hz), 7.52 (d, 2H, *J* = 8.4 Hz), 7.59 (s, 1H), 7.90–7.92 (m, 3H). ^{13}C-NMR (DMSO-d_6, 400 MHz) δ ppm: 21.17, 21.81, 47.33, 54.16, 62.19, 115.60, 122.64, 126.39, 128.23, 128.26, 129.61, 129.86, 131.30, 131.83, 132.29, 134.10, 138.97, 145.18, 160.07, 166.69, 189.37 M.F: $C_{30}H_{26}N_4O_4S$. HRMS *m*/*z* (ES+): $[M + H]^+$ 539.1675 (539.1693). Purity %: 99.93.

2.2.9. 5-(4-((1-(4-Methoxybenzyl)-1*H*-1,2,3-triazol-4-L)methoxy)benzylidene)-3-(2-oxo-2-(P-tolyl)ethyl)thiazolidine-2,4-dione (**SDP9**)

White powder, m.p: 208–210 °C, yield: 64, R_f: 0.59: IR (KBr, ν_{max}, cm^{-1}): 3006 (C-H), 2935–2838 (C-H), 1675 (C=O), 1513 (C=C); ^{1}H-NMR ($CDCl_3$; 400 MHz) δ ppm: 2.47 (s, 3H, -CH_3), 3.84 (s, 3H, -OCH_3), 5.17 (s, 2H, -CH_2-), 5.26 (s, 2H, -CH_2-), 5.50 (s, 2H, -CH_2-), 6.94 (d, 2H, *J* = 8.8 Hz), 7.11 (d, 2H, *J* = 8.8 Hz), 7.26 (d, 2H, *J* = 8.8 Hz), 7.35 (d, 2H, *J* = 8 Hz), 7.53 (d, 2H, *J* = 8 Hz), 7.50 (s, 1H), 7.90–7.92 (m, 3H). ^{13}C-NMR (DMSO-d_6, 400 MHz) δ ppm: 21.81, 47.33, 53.91, 55.37, 62.20, 100.71, 114.56, 115.60, 128.26, 129.61, 132.29, 134.09, 145.20, 159.03, 160.07. M.F: $C_{30}H_{26}N_4O_5S$. HRMS *m*/*z* (ES+): $[M + H]^+$ 555.1624 (555.1716). Purity %: 99.92.

2.2.10. 5-(4-((1-(4-Chlorophenyl)-1*H*-1,2,3-triazol-4-Yl)methoxy)benzylidene)-3-(2-oxo-2-(P-tolyl)ethyl)thiazolidine-2,4-dione (**SDP10**)

White crystalline powder, m.p: 215–217 °C, yield: 66, Rf: 0.68: IR (KBr, ν_{max}, cm^{-1}): 3157–3014 (C-H), 2975–2870 (C-H), 1676(C=O), 1511 (C=C); ^{1}H NMR ($CDCl_3$; 400 MHz) δ ppm: 2.47 (s, 3H, -CH_3), 5.17 (s, 2H, -CH_2-), 5.28 (s, 2H, -CH_2-), 5.58 (s, 2H, -CH_2-), 7.12 (d, 2H, *J* = 8.8 Hz), 7.35–7.30 (m, 4H), 7.38–7.44 (m, 3H), 7.52 (d, 2H, *J* = 8.8 Hz), 7.61 (s,

1H), 7.92 (d, 3H, *J* = 8.0 Hz).^{13}C-NMR (DMSO-d_6, 400 MHz) δ ppm: 21.81, 47.33, 54.35, 62.18, 115.60, 118.80, 122.76, 126.41, 128.16, 128.26, 128.92, 129.21, 129.61, 131.82, 132.29, 134.08, 134.35, 143.85, 145.21, 160.08, 166.10, 167.84, 189.38. M.F: $C_{29}H_{23}ClN_4O_4S$. HRMS *m*/*z* (ES+): $[M + H]^+$ 559.1129 (559.1141). Purity %: 84.23.

2.2.11. 3-(2-(4-Bromophenyl)-2-oxoethyl)-5-(4-((1-(4-nitrobenzyl)-1*H*-1,2,3-triazol-4-Yl)methoxy)benzylidene)thiazolidine-2,4-dione (**SDP11**)

White crystalline powder, m.p: 235–237 °C, yield: 72, R_f: 0.59: IR (KBr, ν_{max}, cm^{-1}): 3081 (C-H), 2975–2877(C-H), 1683 (C=O), 1518 (C=C); ^{1}H-NMR ($CDCl_3$; 400 MHz) δ ppm:5.15 (s, 2H, -CH_2-), 5.28 (s, 2H, -CH_2-), 5.54 (s, 2H, -CH_2-), 7.12 (d, 2H, *J* = 8.8 Hz), 7.26 (d, 2H, *J* = 8.4 Hz), 7.40 (d, 2H, *J* = 8.4 Hz), 7.52 (d, 2H, *J* = 8.8 Hz), 7.58 (s, 1H), 7.70 (d, 2H, *J* = 8.4 Hz), 7.88 (d, 2H, *J* = 8.4 Hz), 7.91 (s, 1H). ^{13}C-NMR (DMSO-d_6, 400 MHZ) δ ppm: 48.28, 52.53, 61.83, 116.25, 118.16, 125.44, 126.08, 129.17, 129.26, 130.41, 130.79, 132.61, 132.88, 133.29, 133.38, 134.34, 135.44, 142.99, 147.66, 160.57, 165.76, 167.51, 191.34. M.F: $C_{28}H_{20}BrN_5O_6S$. HRMS *m*/*z* (ES+): $[M + H]^+$ 634.0318 (634.0352). Purity %: 99.80.

2.2.12. 5-(4-((1-Benzyl-1*H*-1,2,3-triazol-4-Yl)methoxy)benzylidene)-3-(2-(4-bromophenyl)-2-oxoethyl)thiazolidine-2,4-dione (**SDP12**)

White crystals, m.p: 212–214 °C, yield: 67, R_f: 0.58: IR (KBr, ν_{max}, cm^{-1}): 3138–3019 (C-H), 2955–2872 (C-H), 1682 (C=O), 1511 (C=C); ^{1}H-NMR ($CDCl_3$; 400 MHz) δ ppm: 5.15 (s, 2H, -CH_2-), 5.31 (s, 2H, -CH_2-), 5.70 (s, 2H, -CH_2-), 7.13 (d, 2H, *J* = 8.8 Hz, Ar), 7.46 (d, 2H, *J* = 8.4 Hz), 7.53 (d, 2H, *J* = 8.8 Hz), 7.66 (s, 1H), 7.71 (d, 2H, *J* = 8.4 Hz), 7.89 (d, 2H, *J* = 8.4 Hz), 7.92 (s, 1H), 8.28 (d, 2H, *J* = 8.8 Hz). M.F: $C_{28}H_{21}BrN_4O_4S$. HRMS *m*/*z* (ES+): $[M + H]^+$ 589.0467 (589.0596). Purity %: 99.99.

2.2.13. 3-(2-(4-Bromophenyl)-2-oxoethyl)-5-(4-((1-(4-methylbenzyl)-1*H*-1,2,3-triazol-4-Yl)methoxy)benzylidene)thiazolidine-2,4-dione (**SDP13**)

White crystals, m.p: 206–208 °C, yield: 69, R_f: 0.61: IR (KBr, ν_{max}, cm^{-1}): 3141–3019 (C-H), 2922–2874 (C-H), 1682 (C=O), 1511(C=C); ^{1}H-NMR ($CDCl_3$; 400 MHz) δ ppm:2.38 (s, 3H, -CH_3), 5.15 (s, 2H, -CH_2-), 5.26 (s, 2H, -CH_2-), 5.52 (s, 2H, -CH_2-), 7.11 (d, 2H, *J* = 8.8 Hz), 7.21 (s, 4H), 7.51 (d, 2H, *J* = 8.8 Hz), 7.55 (s, 1H), 7.70 (d, 2H, *J* = 8.8 Hz), 7.88 (d, 2H, *J* = 8.8 Hz), 7.90 (s, 1H). ^{13}C-NMR (DMSO-d_6, 400 MHz) δ ppm: 21.17, 47.23, 54.15, 62.19, 115.63, 118.52, 122.68, 126.28, 128.22, 129.54, 129.60, 129.86, 131.31, 132.33, 133.01, 134.36, 138.90, 143.70, 160.21, 165.96, 167.76, 189.05. M.F: $C_{29}H_{23}BrN_4O_4S$. HRMS *m*/*z* (ES+): $[M + H]^+$ 603.0623 (603.0699). Purity %: 99.96.

2.2.14. 3-(2-(4-Bromophenyl)-2-oxoethyl)-5-(4-((1-(4-methoxybenzyl)-1*H*-1,2,3-triazol-4-Yl)methoxy)benzylidene)thiazolidine-2,4-dione (**SDP14**)

White amorphous powder, m.p: 202–204 °C, yield: 70, R_f: 0.64: IR (KBr, ν_{max}, cm^{-1}): 3141–3019 (C-H.), 2922–2874 (C-H), 1682 (C=O), 1511 (C=C); ^{1}H-NMR (DMSO-d_6; 400 MHz) δ ppm: 3.74 (s, 3H, -OCH_3), 5.24 (s, 2H, -CH_2-), 5.33 (s, 2H, -CH_2-), 5.54 (s, 2H, -CH_2-), 6.95 (d, 2H, *J* = 8.8 Hz), 7.25 (d, 2H, *J* = 8.8 Hz), 7.32 (d, 2H, *J* = 8.8 Hz), 7.67 (d, 2H, *J* = 8.8 Hz), 7.85 (d, 2H, *J* = 8.8 Hz), 7.98 (s, 1H), 8.04 (d, 2H, *J* = 8.8 Hz), 8.28 (s, 1H). ^{13}C-NMR (DMSO-d_6, 400 MHZ) δ ppm:47.22, 53.91, 55.36, 62.20, 114.57, 115.64, 122.53, 126.26, 129.59, 129.77, 132.34, 134.37, 160.07, 165.97, 189.02. M.F: $C_{29}H_{23}BrN_4O_5S$. HRMS *m*/*z* (ES+): $[M + H]^+$ 619.0573 (619.0707). Purity %: 99.93.

2.2.15. 3-(2-(4-Bromophenyl)-2-oxoethyl)-5-(4-((1-(4-chlorobenzyl)-1*H*-1,2,3-triazol-4-Yl)methoxy)benzylidene)thiazolidine-2,4-dione (**SDP15**)

White crystals, m.p: 251–253 °C, yield: 61, R_f: 0.61: IR (KBr, ν_{max}, cm^{-1}):3137–3019(C-H, ar.), 2955–2874 (C-H), 1681(C=O), 1511 (C=C); ^{1}H-NMR ($CDCl_3$; 400 MHz) δ ppm: 5.15 (s, 2H, -CH_2-), 5.28 (s, 2H, -CH_2-), 5.57 (s, 2H, -CH_2-), 7.12 (d, 2H, *J* = 8.8 Hz), 7.29–7.32 (m,

2H), 7.40–7.42 (m, 3H), 7.52 (d, 2H, *J* = 8.8 Hz), 7.57 (s, 1H), 7.70 (d, 2H, *J* = 8.4 Hz), 7.89 (d, 2H, *J* = 8.8 Hz), 7.91 (s, 1H). ^{13}C-NMR (DMSO-d_6, 400 MHz) δ ppm: 47.23, 54.35, 62.19, 115.64, 118.56, 122.78, 126.31, 128.16, 128.92, 129.21, 129.54, 129.60, 132.34, 133.01, 134.34, 143.34, 160.18, 165.96, 167.76, 189.04. M.F: $C_{28}H_{20}BrClN_4O_4S$. HRMS *m*/*z* (ES+): $[M + H]^+$ 623.0077 (623.0026). Purity %: 99.29.

2.3. Biological Investigations

2.3.1. Antidiabetic Activity (In Vitro Enzyme Inhibition)

α-Amylase Inhibition Assay

The invitroα-amylase inhibition assay is used for evaluating the antidiabetic potential of a molecule. Typically, it is performed by the DNA (3,5-dinitrosalicylic acid) method. Briefly, a reaction mixture containing PBS (phosphate buffer) pH 6.8, α-amylase, and varying concentrations of the test compounds (final volume up to 100 µL) was pre-incubated at 37 °C for about 10 min. Subsequently, a starch solution was added, and the mixture was incubated further for enzymatic hydrolysis. The reaction was terminated by adding DNSA reagent, followed by heating in a boiling water bath for approximately 5 min to develop color. After cooling, the absorbance was measured at 540 nm. The degree of inhibition was calculated by comparing the absorbance of the test sample with that of the control, and the % (percentage)inhibition was determined using the standard Formula (1). The IC_{50} values (in µg/mL) were obtained by plotting percentage inhibition against different concentrations of the test compound. Acarbose was commonly used as a positive control during the study [25].

$$\text{Inhibition}(\%) = \text{Ac} - \text{As}/\text{Ac} \times 100 \quad (1)$$

where:

Ac = Absorbance of control.

As = Absorbance with sample.

α-Glucosidase Inhibition Assay

The α-glucosidase inhibition assay is performed to evaluate the delayed carbohydrate digestion and reduction in postprandial blood glucose spikes. Briefly, 50 µL of α-glucosidase solution (1 U/mL) was prepared in 50 mM PBS (pH 6.9). To this, varying concentrations of the test compounds (**SDP1–SDP15**) were added (final volume up to 100 µL), and the reaction mixture was pre-incubated at 37 °C for 10 min, followed by the addition of 50 µL of pNPG (p-nitrophenyl-α-D-glucopyranoside, 5 mM) as the substrate and further incubation at 37 °C for 20 min. The reaction was terminated by adding 1 Molar of aqueous Na_2CO_3 (sodium carbonate) solution, which also facilitated the development of a yellow color due to the release of p-nitrophenol. The absorbance was measured at 405 nm. The percentage inhibition was calculated by comparing the absorbance of test samples with that of the control, as per Formula (1). The IC_{50} values (in µg/mL) were obtained by plotting percentage inhibition against different concentrations of the test compound. Acarbose and pioglitazone were used as positive controls during the study [26].

2.3.2. Molecular Docking and ADME Calculation

The protein–ligand (reference and target molecules) interactions were performed using the Autodock VinaPyRx program (version 0.8). The docking method had previously been established [27,28]. In brief, α-glucosidase protein (PDB ID: 3TOP) and α-amylase (PDB ID: 1B2Y) were extracted from the PDB. The ligand structures (two- and three-dimensional) were drawn using Chem Draw Ultra 12 and modified in 3D conformers. The protein was treated before being saved in PDBQT format, which included eliminating excess metals and water, reducing energy, and introducing hydrogen to the native ligand. The ligand

was altered by reducing its energy content level and introducing Gasteiger charges and polar hydrogen. The file was saved using PDBQT, with active torsion set to 6. The grid box for α-amylase was created using center attributes (X = 20.25, Y = 8.74, Z = 49.26) and size (X = 25, Y = 25, and Z = 25). The grid box for α-glucosidase was created using center attributes (X = 29.03, Y = 35.95, Z = 26.74) and size (X = 25, Y = 25, and Z = 25). The number of conformers was set at ten with an exhaustiveness of eight. The interaction was presented with the Discovery Studio visualization software (version 4). The docking scores were captured, and the 3D contact photos were stored as JPG files at a resolution of 500 dpi. An in-silico ADME study was performed on Swiss-ADME [29].

2.4. pH Solubility Profiling

The solubility of **SDP8** at pH 7.4 was evaluated using phosphate buffer pH 7.4. Excess **SDP8** (5 mg) was added to 2 mL of phosphate buffer pH 7.4 in tightly stoppered glass vials and equilibrated under continuous agitation using an orbital shaker at room temperature for 24h to attain saturation equilibrium. Following equilibration, the dispersions were filtered through Whatman filter paper No. 42 (0.45 µm pore size) to separate the undissolved drug. The filtrates were suitably diluted with phosphate buffer pH 7.4 and analyzed spectrophotometrically at 334 nm using a Shimadzu 1900i UV–visible spectrophotometer (Kyoto, Japan), with phosphate buffer pH 7.4 used as the blank. The concentration of dissolved **SDP8** was calculated using the previously constructed calibration curve [30]. All experiments were performed in triplicate, and the results were expressed as mean ± standard deviation.

2.5. Determination of pH–Log P Profile

The partition coefficient (P) of **SDP8** was determined using the differential shake-flask method employing n-octanol and phosphate buffer pH 7.4 to evaluate its lipophilic behavior. **SDP8** (5 mg) was dispersed in a biphasic system containing 2mL of phosphate buffer pH 7.4 and 2 mL of n-octanol in tightly stoppered glass vials. The mixtures were equilibrated under continuous agitation using an orbital shaker at room temperature for 24h to attain partition equilibrium between the aqueous and organic phases. Following equilibration, the phases were separated by centrifugation at 2000 rpm for 10 min. An aliquot of the aqueous phase was carefully withdrawn, filtered through a 0.45 µm membrane filter, suitably diluted with phosphate buffer pH 7.4, and analyzed spectrophotometrically at 334 nm using a Shimadzu 1900i UV–visible spectrophotometer (Kyoto, Japan). The concentration of **SDP8** in the aqueous phase was determined using the previously constructed calibration curve, while the concentration in the octanol phase was calculated indirectly [31]. The partition coefficient (P) was calculated using Equation (2).

$$P = \frac{C_{oct}}{C_{aq}} \quad (2)$$

where C_{oct} and C_{aq} denote the equilibrium concentrations of **SDP8** in the n-octanol and aqueous buffer phases, respectively. All determinations were carried out in triplicate, and the results were expressed as mean values.

3. Results and Discussion

3.1. Chemistry

Synthesis of triazole-linked thiazolidinedione hybrids (**SDP1–SDP15**) was carried out as shown in Scheme 1. Briefly, 2,5-Thazolidindione (**1**) was reacted with different phenacyl bromides (**2a–c**) to yield *N*-substituted thiazolidindiones (**3a–c**). Subsequently, 4-(prop-2-nyloxy)benzaldehyde (**6**) was obtained by a reaction between 4-hydroxy benzaldehyde (**4**) and propargyl bromide (**5**) in DMF and anhydrous potassium carbonate.

Different p-substituted benzyl azides (**9a–e**) were prepared by reacting p-substituted benzyl chlorides (**7a–e**) and sodium azide (**8**) in a mixture of acetone and water. Different triazole-aldehydes (**10a–e**) were prepared by reacting 4-(prop-2-yn-1-yloxy) benzaldehyde (**6**) and p-substituted benzyl azides (**9a–e**) in the presence of $CuSO_4 \cdot 5H_2O$, sodium ascorbate, and *tert*-butanol. The final step involved the synthesis of *N*-substituted 5-arylidine-thiazolidinedione (**SDP1–SDP15**), involving a reaction between *N*-substituted thiazolidindiones (**3**) with respective triazole-aldehydes (**10a–e**). All derivatives (**SDP1–SDP15**) were recrystallized with ethanol and DMF mixture.

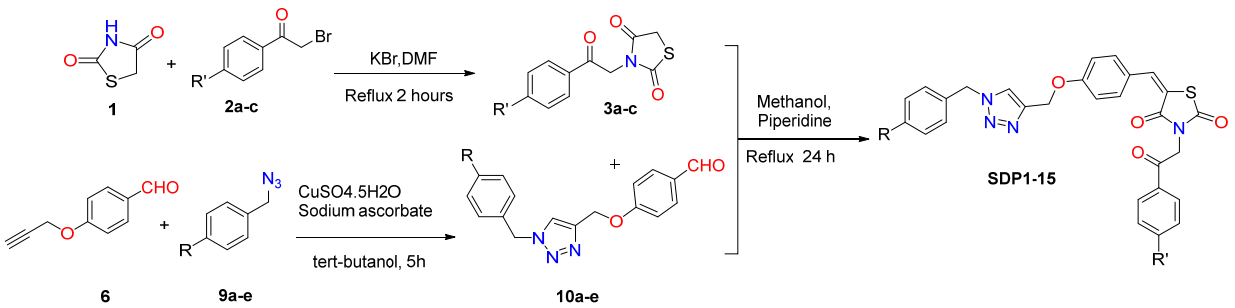

Scheme 1. Synthesis of *p*-substituted-5-(4-((1-benzyl-1*H*-1,2,3-triazol-4-yl)methoxy)benzylidene)-3-(2-oxo-2-phenylethyl) thiazolidine-2,4-dione (**SDP1–SDP15**).

3.2. Biological Evaluation

3.2.1. In Vitro α-Amylase and α-Glucosidase Inhibition

The α-amylase and α-glucosidase inhibitory activities of the synthesized derivatives (**SDP1–SDP15**) were evaluated using acarbose and pioglitazone as positive controls. The compounds exhibited promising inhibitory activity, with IC_{50} values ranging from 26–46.41 µg/mL for α-glucosidase and 23.25–50.66 µg/mL for α-amylase. Acarbose showed IC_{50} values of 25.18 µg/mL (α-glucosidase) and 32.53 µg/mL (α-amylase), whereas pioglitazone displayed comparatively weaker inhibition of 84.24 and 79.74 µg/mL for α-glucosidase and α-amylase, respectively. Structure–activity relationship (SAR) analysis highlighted the influence of benzyl and phenacyl substitutions on the triazole-thiazolidinedione scaffold. **SDP2**, and **SDP7** (*p*-chlorobenzyl) were equipotent to acarbose against α-glucosidase, while electron-donating substituents such as p-methyl (**SDP3**), p-methoxy (**SDP4**), and unsubstituted benzyl (**SDP1**) exhibited moderate activity against α-glucosidase and α-amylase. In contrast, the bulky electron-withdrawing p-nitro group in **SDP5**, **SDP10**, and **SDP15** exhibited reduced inhibition of both enzymes. Introduction of a methyl group on the phenacyl ring has exhibited a mixed response on enzyme inhibition. For example, molecules **SDP4**, **SDP8,** and **SDP9** have exhibited enhanced inhibition against α-amylase, while **SDP3**, **SDP13**, and **SDP14** failed to do so. Notably, **SDP8** (*p*-methyl substitution on both benzyl and phenacyl rings) emerged as the most potent compound, showing superior α-glucosidase inhibition (IC_{50} = 24.17 µg/mL), approximately 3.48-fold more active than pioglitazone, and strong α-amylase inhibition. Substitution of the phenacyl ring with electron-withdrawing bromo moiety (**SDP11–SDP15**) led to reduced activity, although **SDP12** had shown some selectivity toward α-amylase. Overall, electron-donating substituents on both benzyl and phenacyl rings significantly enhanced inhibitory activity, whereas electron-withdrawing groups diminished potency. Further, except for **SDP8** and **SDP11**, the rest of the molecules were found to be moderate or less potent inα-amylase inhibition compared to acarbose. It was also noted that, irrespective of substitution, the IC_{50} of all molecules was found to be better than the reference molecule pioglitazone against α-glucosidase and α-amylase enzymes, demonstrating their possible antidiabetic property (Table 1).

Table 1. Invitroα-amylase and α-glucosidase inhibitory activity.

Sl. No.	Compounds	α-Glucosidase IC_{50} (µg/mL)	α-Amylase IC_{50} (µg/mL)
1	**Acarbose**	25.18	32.53
2	**Pioglitazone**	84.24	79.74
3	**SDP1**	30.06	37.41
4	**SDP2**	26.00	37.41
5	**SDP3**	46.41	50.66
6	**SDP4**	29.27	41.80
7	**SDP5**	33.29	42.58
9	**SDP6**	30.12	28.10
12	**SDP7**	26.31	40.25
11	**SDP8**	24.17	23.25
12	**SDP9**	27.58	38.15
13	**SDP10**	28.88	30.42
14	**SDP11**	38.54	25.00
15	**SDP12**	43.79	47.73
16	**SDP13**	38.22	37.68
17	**SDP14**	34.19	34.19
18	**SDP15**	33.92	48.25

Overall, the biological evaluation clearly demonstrates that the produced compounds' antidiabetic action is predominantly achieved by enzyme inhibition. All substances showed considerable inhibitory effects against α-amylase and α-glucosidase, with some analogues displaying equivalent or greater efficacy to the conventional medication acarbose and consistently outperforming pioglitazone. The observed SAR patterns add to the evidence for this mechanism, as specific substitutions had a systematic effect on enzyme inhibitory potency. Notably, **SDP8** emerged as the most active molecule, confirming enzyme inhibition as the series' dominant and empirically proven mode of action, whereas any additional mechanistic insights are secondary and require further exploration.

3.2.2. Molecular Docking Analysis

Inhibition of α-Glucosidase

The synthesized compounds (**SDP1–SDP15**) were evaluated for binding affinity to the α-glucosidase enzyme using acarbose and pioglitazone as reference standards. The synthesized compounds have docking scores ranging from −6.2 to −10.7 kcal/mol, indicating moderate to excellent interaction with α-glucosidase's active site. Among testing, **SDP8** had the highest binding affinity, with a docking score of −10.7 kcal/mol, surpassing standard drugs acarbose (−10.4 kcal/mol) and pioglitazone (−8.1 kcal/mol). Compounds **SDP2** (−10.5 kcal/mol), **SDP7** (−10.4 kcal/mol), **SDP9** (−10.3 kcal/mol), and **SDP10** (−10.2 kcal/mol) showed comparable or superior docking affinity to acarbose, indicating considerable inhibitory potential against α-glucosidase. Furthermore, **SDP4** (−9.7 kcal/mol) and **SDP1** (−9.3 kcal/mol) had a positive interaction with the enzyme. **SDP6** and **SDP14** (−8.7 kcal/mol each), **SDP13** (−8.5 kcal/mol), and **SDP5** and **SDP15** (−8.4 kcal/mol each) had moderate binding affinity, with docking scores better than or equivalent to pioglitazone. **SDP11** (−7.4 kcal/mol), **SDP12** (−6.9 kcal/mol), and **SDP3** (−6.2 kcal/mol) had lower binding affinity for α-glucosidase. Overall, the docking study revealed that the majority of the synthesized derivatives had a promising contact with the enzyme active site, with **SDP8** emerging as the most powerful compound in the series for further biological evaluation and mechanistic antidiabetic research (Table 2). The molecular docking results against α-glucosidase were found to be in good agreement with the in vitro biological evaluation. Compounds showing stronger docking affinity, particularly **SDP8**,

SDP2, **SDP7**, **SDP9**, and **SDP10**, also demonstrated lower IC_{50} values in the enzymatic assay, indicating better antidiabetic activity. Conversely, compounds with weaker docking scores such as **SDP3** and **SDP12** exhibited comparatively lower biological potency. The observed correlation between docking and experimental findings suggests that the synthesized compounds may exert their antidiabetic activity through inhibition of the α-glucosidase enzyme.

Table 2. Docking scores of synthesized compounds against α-glucosidase.

Compound	α-Glucosidase Dock Score (Kcal/mol)
Acarbose	−10.4
Pioglitazone	−8.1
SDP 1	−9.3
SDP 2	−10.5
SDP 3	−6.2
SDP 4	−9.7
SDP 5	−8.4
SDP 6	−8.7
SDP 7	−10.4
SDP 8	−10.7
SDP 9	−10.3
SDP 10	−10.2
SDP 11	−7.4
SDP 12	−6.9
SDP 13	−8.5
SDP 14	−8.7
SDP 15	−8.4

Compound **SDP8**, which was identified as the most active molecule in the enzymatic assay against α-glucosidase, was subsequently chosen for a comprehensive molecular docking analysis to elucidate its binding interactions within the active site of the enzyme. The binding pocket of α-glucosidase was discovered to be surrounded by critical residues, such as Trp1355, Trp1369, Phe1427, Tyr1251, Asp1157, Arg1156, Lys1460, Asn1429, and Arg1455. These residues are recognized for their substantial contributions to ligand stabilization through hydrophobic, π–π stacking, and hydrogen bonding interactions.

The docking results indicated that **SDP8** had a binding affinity of −10.7 kcal/mol, suggesting a robust interaction with the enzyme. Within the active compartment, the ligand established numerous stabilizing interactions. It is important to note that the aromatic rings of **SDP8** formed π–π stacking interactions with Trp1355 and Trp1369, and additional hydrophobic contacts were observed with residues such as Phe1427 and Tyr1251. In addition, **SDP8** exhibited key hydrogen bonding interactions with Lys1460, Asn1429, and Arg1455, which are essential for anchoring the ligand within the catalytic site. It appears that the presence of flexible linkers and multiple aromatic systems in **SDP8** enables optimal fitting and extensive interaction with the active site residues, thereby improving binding stability.

In contrast, the standard drug pioglitazone demonstrated a comparatively lower binding affinity of −8.1 kcal/mol, indicating a reduced interaction with α-glucosidase. Pioglitazone primarily formed hydrogen bonds with Arg1510 and His1584, as well as limited π–π interactions involving Trp1355, according to the interaction analysis. Although hydrophobic interactions were observed with residues such as Tyr1251 and Phe1559, the overall interaction network was less extensive than that of **SDP8**.

The relatively smaller scaffold and limited aromatic surface of pioglitazone may be responsible for its comparatively reduced binding affinity. These factors limit its capacity to establish extensive π–π stacking and hydrophobic interactions within the active site. In contrast, **SDP8**, due to its more structurally diverse and expansive framework, is capable of establishing multiple simultaneous interactions and occupying a larger portion of the binding region (Figures 2 and 3).

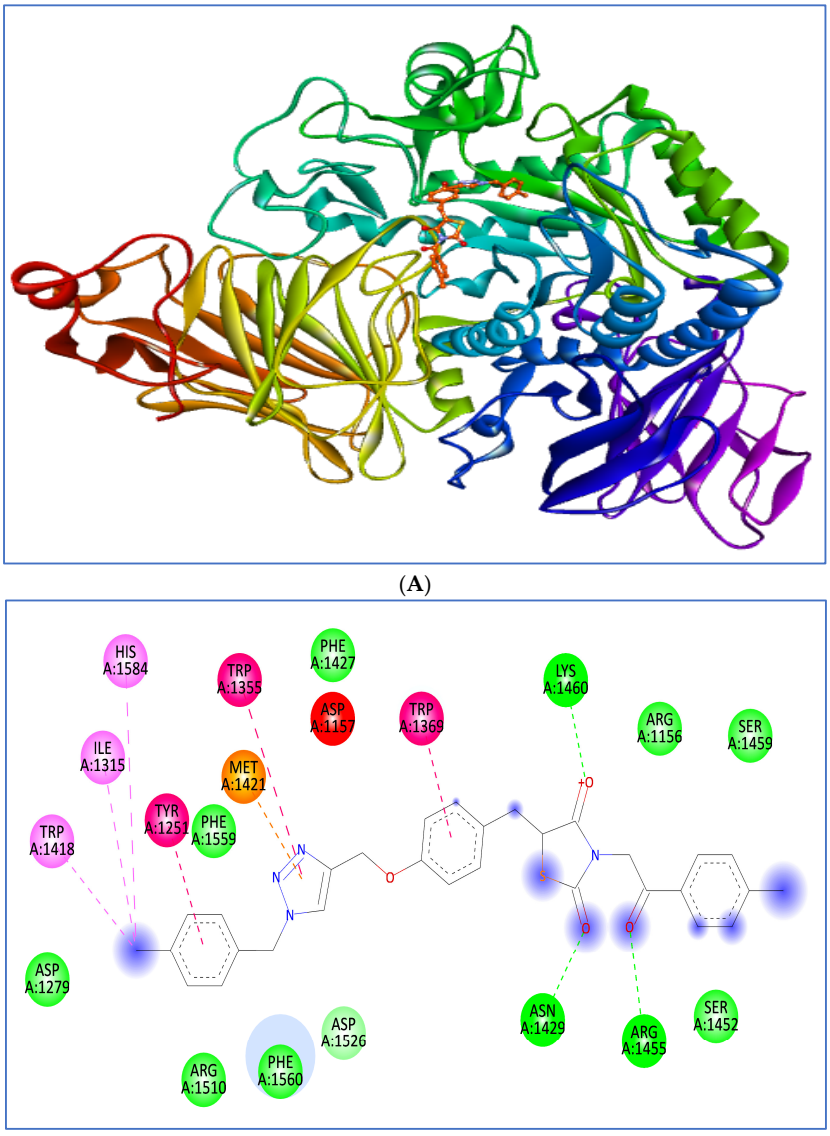

Figure 2. Docking interaction images of **SDP8** against α-glucosidase: (**A**) Three-dimensional ribbon representation illustrating the binding pose of SDP8 within the active-site cavity. (**B**) Two-dimensional interaction map showing the key protein–ligand interactions. Conventional hydrogen bonds are represented by green dashed lines, lipophilic interactions by gray dashed lines, π–π T-shaped interactions by pink dashed lines, π–alkyl interactions by light pink dashed lines, and π–cation interactions by orange dashed lines. Amino acid residues are color-coded according to their physicochemical properties, with green circles (light and dark shades) indicating polar residues, pink circle (light and dark shades) indicating hydrophobic residues, red circles negatively charged residuess, and orange circles denoting residues involved in π-cation interactions. Residues surrounded by light blue contours represent van der Waals interactions. The blue contours around ligand atoms represent solvent-accessible regions generated by Discovery Studio Visualizer.

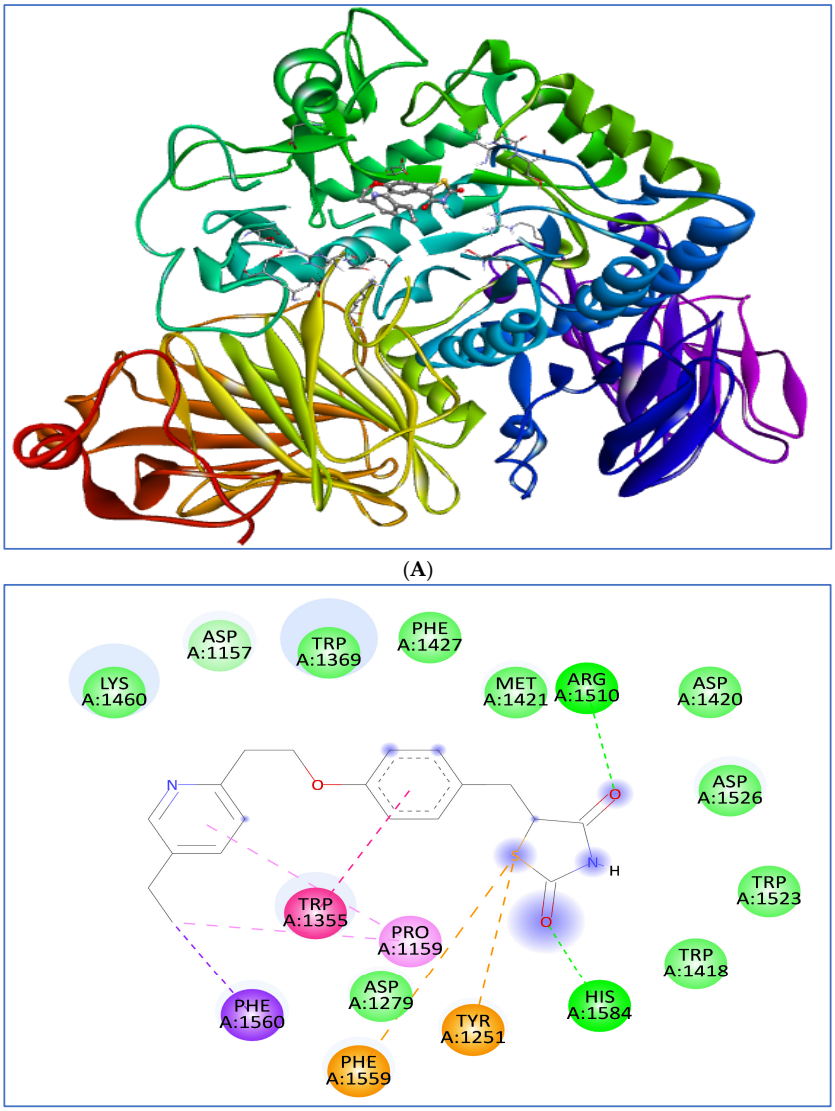

Figure 3. Docking interaction images of pioglitazone against α-glucosidase: (**A**) 3D docking pose of pioglitazone within the catalytic pocket of α-glucosidase represented as a rainbow-colored ribbon model (red-to-violet indicating N- to C-terminal orientation). The ligand is shown in stick representation within the active-site cavity interacting with key residues. (**B**) 2D interaction map showing key interacting amino acid residues. Green dashed lines indicate hydrogen bonds, gray dashed lines indicate lipophilic interactions, pink dashed lines indicate π–π T-shaped interactions, light pink dashed lines indicate π–alkyl interactions, purple dashed lines denote π–π stacked interactions, and orange dashed lines denote π–cation interactions. Amino acid residues are color-coded according to their interaction characteristics, with green circles (light and dark shades) indicating polar residues, pink circles (light and dark shades) indicating hydrophobic residues, purple circles representing aromatic interaction residues, and orange circles denoting residues involved in π-cation interactions. Residues surrounded by light blue contours represent van der Waals interactions. The blue contours around ligand atoms represent solvent-accessible regions generated by Discovery Studio Visualizer.

These findings are in agreement with the enzymatic inhibition study, which implies that **SDP8**'s antidiabetic activity is at least partially mediated by the potent inhibition of α-glucosidase.

α-Amylase Inhibitors

Molecular docking studies against the α-amylase enzyme were performed to evaluate the binding affinity of the synthesized compounds (**SDP1–SDP15**) in comparison

with the standard drugs acarbose and pioglitazone. The docking scores of the synthesized derivatives ranged from −6.9 to −10.4 kcal/mol, indicating moderate to excellent interaction with the target enzyme. Among all tested compounds, **SDP8** exhibited the highest binding affinity with a docking score of −10.4 kcal/mol, followed by **SDP11** (−10.3 kcal/mol), **SDP6** (−10.2 kcal/mol), **SDP10** (−10.0 kcal/mol), **SDP14** (−9.9 kcal/mol), **SDP1** (−9.4 kcal/mol), and **SDP2** (−9.2 kcal/mol), suggesting strong affinity toward the α-amylase active site. Compounds **SDP9** and **SDP13** showed similar docking scores of −8.8 kcal/mol, while **SDP7** (−8.1 kcal/mol), **SDP4** (−7.9 kcal/mol), **SDP5** (−7.7 kcal/mol), **SDP12** (−7.5 kcal/mol), **SDP15** (−7.1 kcal/mol), and **SDP3** (−6.9 kcal/mol) demonstrated moderate to lower binding affinity. **SDP5** exhibited a docking score comparable to pioglitazone (−7.7 kcal/mol), whereas several synthesized compounds showed better binding affinity than the standard drug pioglitazone. Although acarbose displayed the strongest docking score of −16.1 kcal/mol, the synthesized derivatives demonstrated considerable interaction with α-amylase, highlighting their potential as antidiabetic agents. Overall, the docking results suggested that **SDP8** emerged as the most promising compound among the synthesized series for further biological evaluation and mechanistic studies targeting α-amylase inhibition (Table 3). A good correlation was also observed between the α-amylase docking results and the in vitro enzymatic inhibition studies. Compounds exhibiting higher binding affinity toward α-amylase, especially **SDP8**, **SDP6**, **SDP10**, and **SDP11**, showed significant inhibitory activity with lower IC_{50} values in the biological assay. In contrast, compounds with weaker docking interactions such as **SDP3** and **SDP15** displayed comparatively reduced biological activity. These findings support the hypothesis that the synthesized derivatives possess antidiabetic potential through inhibition of the α-amylase enzyme.

Table 3. Docking scores of synthesized compounds against α-amylase.

Compound	α-Amylase Dock Score (Kcal/mol)
Acarbose	−16.1
Pioglitazone	−7.7
SDP1	−9.4
SDP2	−9.2
SDP3	−6.9
SDP4	−7.9
SDP5	−7.7
SDP6	−10.2
SDP7	−8.1
SDP8	−10.4
SDP9	−8.8
SDP10	−10
SDP11	−10.3
SDP12	−7.5
SDP13	−8.8
SDP14	−9.9
SDP15	−7.1

SDP8 was identified as the most potent inhibitor of α-amylase in the biological enzymatic investigation. Consequently, it was subjected to molecular docking analysis to investigate the structural characteristics that contribute to its improved activity. Key active site residues, such as Trp58, Trp59, Tyr62, His101, Asp197, Glu233, Asp300, His201, Ile235, Leu162, and Thr163, were observed to surround the binding compartment of α-amylase. These residues are essential for the catalytic function and stabilization of ligands.

The docking analysis demonstrated that **SDP8** is well-suited to the active site cavity, with a binding affinity of −10.4 kcal/mol, suggesting a robust interaction with the enzyme. The aromatic moieties of **SDP8** exhibited significant π–π stacking interactions with Trp59 and Tyr62, which significantly contributed to the stabilization of the binding. Furthermore, hydrogen bonding interactions were observed with Thr163 and Asp197, and polar contacts with His201 added to the support for ligand anchoring. The **SDP8**–enzyme complex's overall stability was also influenced by hydrophobic interactions with residues such as Leu162 and Ile235. **SDP8**'s optimal accommodation within the binding region is facilitated by the presence of flexible linkers and multiple aromatic rings, which facilitate extensive interactions with catalytic residues.

On the other hand, pioglitazone demonstrated a lower binding affinity of −7.7 kcal/mol, which implies a relatively weakened interaction with α-amylase. The standard engaged predominantly in hydrogen bonding interactions with Gln63 and His305, as well as in limited π–π interactions involving Tyr62. Although some hydrophobic contacts with Leu162, Ile235, and Tyr151 were observed, the interaction network was less extensive than that of **SDP8**, suggesting that the enzyme's catalytic compartment has a reduced binding stability (Figures 4 and 5).

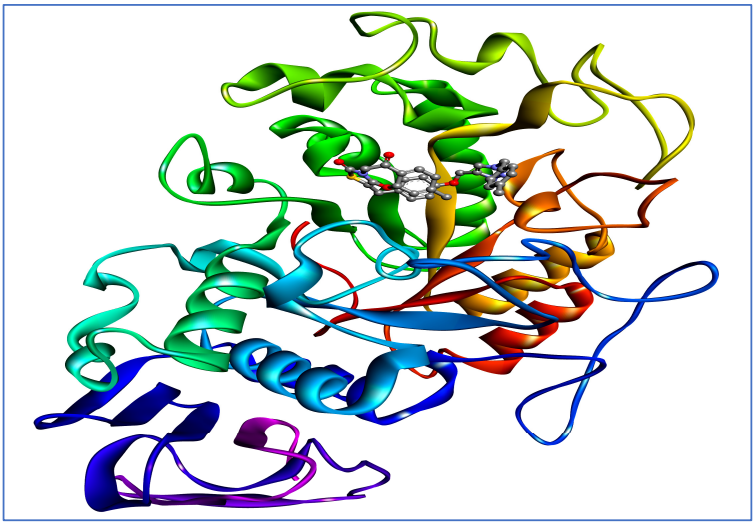

(**A**)

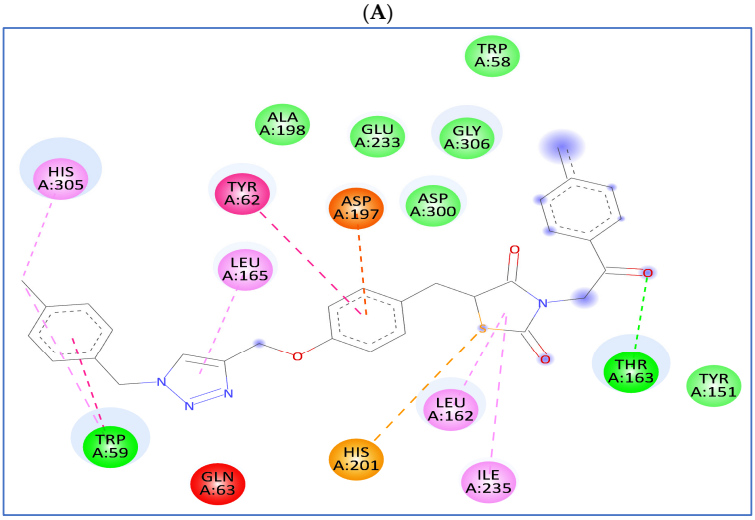

(**B**)

Figure 4. Docking interaction images of **SDP8** against α-amylase: (**A**) 3D ribbon representation of the α-glucosidase–ligand complex showing the binding orientation of the docked compound within the active-site cavity. The rainbow color gradient of the protein ribbon corresponds to the N-terminal to

C-terminal arrangement of the enzyme structure, while the ligand is represented in stick model interacting with surrounding active-site residues. (**B**) 2D interaction diagram illustrating the binding interactions of the docked ligand with amino acid residues present in the active-site pocket of α-amylase. Conventional hydrogen bonds are represented by green dashed lines, lipophilic interactions by gray dashed lines, π–π T-shaped interactions by dark pink dashed lines, π–alkyl interactions by light pink dashed lines, and π–cation interactions by orange dashed lines (light and dark shades). Amino acid residues are color-coded according to their physicochemical properties, with green circles (light and dark shades) indicating polar residues, pink circles (light and dark shades) indicating hydrophobic residues, orange circles (light and dark shades) indicating positively charged, and red circles indicating negatively charged residues. Residues surrounded by light blue contours represent van der Waals interactions. The blue contours around ligand atoms represent solvent-accessible regions generated by Discovery Studio Visualizer.

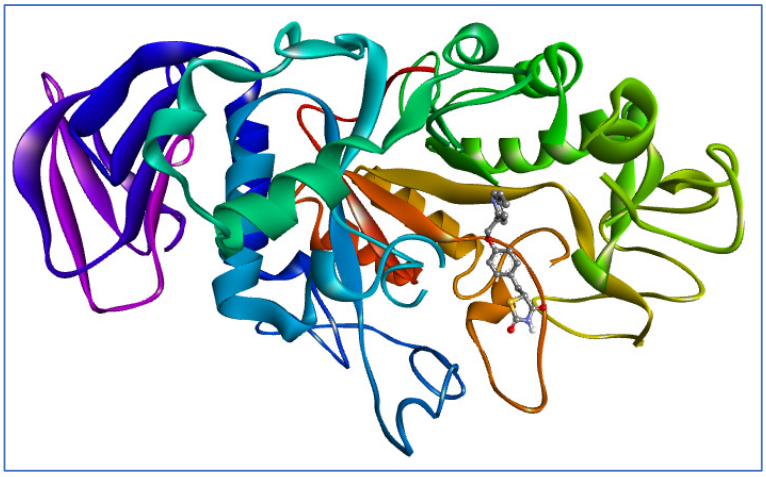

(**A**)

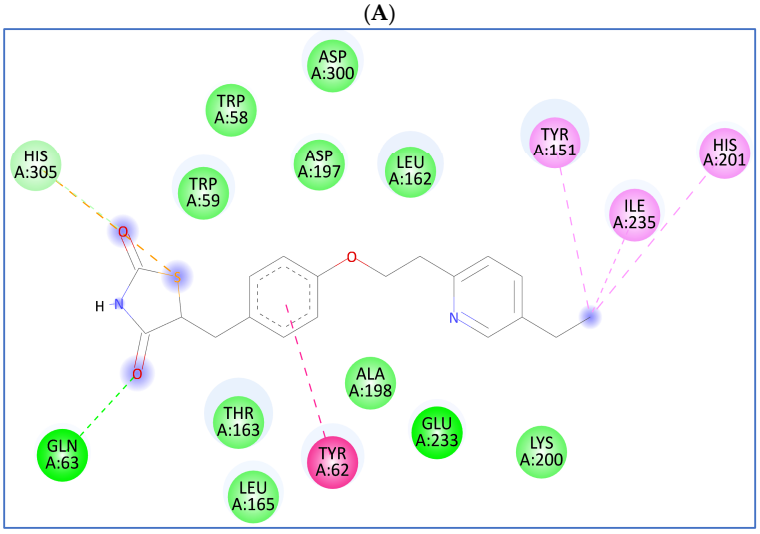

(**B**)

Figure 5. Molecular docking interaction of pioglitazone with α-amylase. (**A**) 3D ribbon/cartoon representation of the protein–ligand docking complex showing the binding orientation of the docked compound within the catalytic active-site cavity. The rainbow-colored protein structure represents the N-terminal to C-terminal arrangement of the enzyme, while the ligand is displayed in stick representation interacting with surrounding active-site amino acid residues through multiple non-covalent interactions. (**B**) 2D molecular interaction diagram of pioglitazone within the α-amylase active-site cavity showing interactions with surrounding amino acid residues. Green dashed lines represent conventional hydrogen-bond interactions, lipophilic interactions by gray dashed lines, π–π T-shaped interactions by pink dashed lines, π–alkyl interactions by light pink dashed lines, while orange dashed lines denote π–cation interactions with key active-site residues. Amino acid residues

are color-coded according to their physicochemical properties, with green circles (light and dark shades) indicating polar residues and pink circles (light and dark shades) indicating hydrophobic residues. Residues surrounded by light blue contours represent van der Waals interactions. The blue contours around ligand atoms indicate solvent-accessible regions generated by Discovery Studio Visualizer.

3.2.3. Density Functional Theory (DFT) Analysis

The potent compound was evaluated for DFT study of its electronic properties. It had the lowest gas-phase energy of −2076.97 eV, indicating stable molecular configurations. The electrostatic potential (ESP) values highlight regions of high electron density, with compound **SDP8** displaying the most negative ESP value (−40.28 kcal/mol), suggesting pronounced electron-rich regions.

The quantum chemical properties of the synthesized derivatives were also examined, including the molecular electrostatic potential (MEP) surface. Frontier molecular orbitals (FMOs), the highest occupied (HOMO), and lowest unoccupied (LUMO) orbitals were analyzed to gauge molecular reactivity and stability. The HOMO–LUMO energy gap (ΔE_{GAP}), shown in Figure 6, is a key reactivity metric: smaller gaps indicate higher reactivity. Compound **SDP8** displayed the smallest gaps (0.1358 eV and 0.1351 eV, respectively), indicating they are more reactive than the other derivatives.

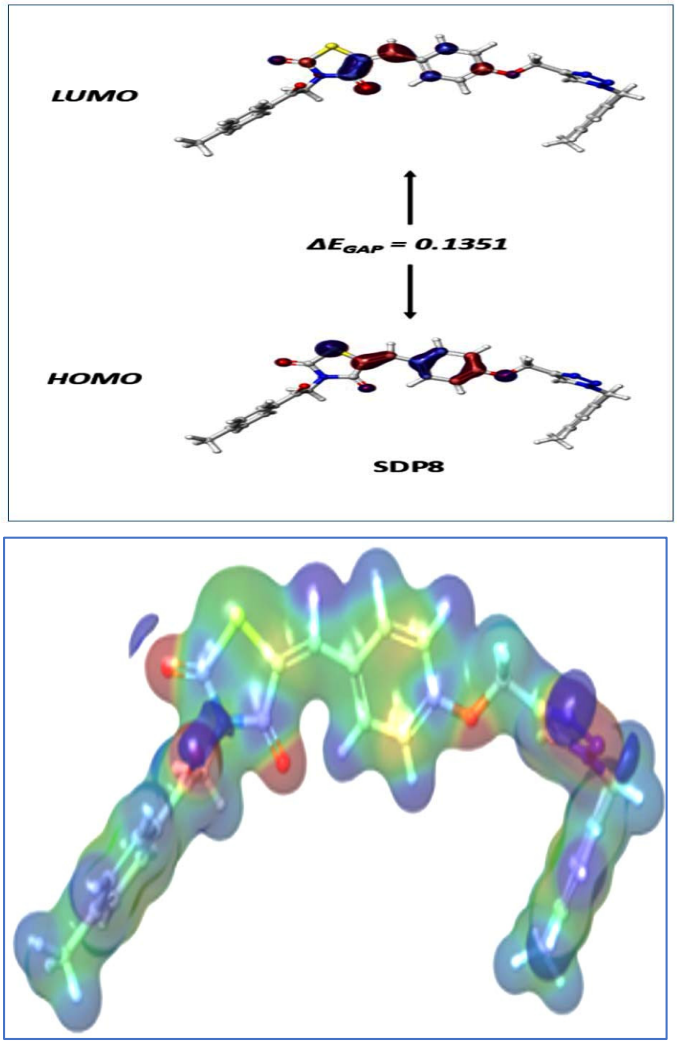

Figure 6. HOMO–LUMO orbitals and the energy gap (ΔE) values of **SDP8**.

The molecular hardness (η), which is inversely related to reactivity, was calculated to be 0.0675 eV, confirming that the compound was relatively soft and thus more reactive. The dipole moment (μ) values, reflecting molecular polarity, were found to be −0.1458 Debye. Additionally, the polarizability (σ) values were nearly identical, indicating comparable polarizability in their values.

The corresponding HOMO and LUMO orbital distributions are illustrated in the FMO framework, where a smaller HOMO–LUMO gap correlates with enhanced reactivity. Notably, compound **SDP8** emerged as the most reactive candidate, exhibiting the lowest hardness value and the smallest ΔE_{GAP} (0.1351 eV). The ESP maps further validate regions favorable for nucleophilic and electrophilic interactions, providing valuable insight into molecular behavior and guiding future investigations into their reactivity.

3.2.4. ADMET Predictions

The ADME analysis of **SDP8** indicates that the compound possesses moderate drug-like characteristics but also exhibits several limitations that may affect its pharmacokinetic performance. The compound shows relatively high lipophilicity (iLOGP = 3.84; XLOGP = 5.38) and a moderate bioavailability score (0.55), suggesting the potential for gastrointestinal absorption. However, the high topological polar surface area (TPSA = 119.69 $Å^2$) and poor aqueous solubility (logS = −6.41) may limit its permeability and dissolution, which are critical for efficient oral absorption.

In addition, **SDP8** shows deviations from established drug-likeness criteria, including one Lipinski violation, two Ghose violations, and one Muegge violation, indicating partial non-compliance with ideal pharmacokinetic properties. The absence of Veber violations suggests acceptable molecular flexibility and polarity, although the predicted low skin permeability (logKp = −5.77 cm/s) further reflects limited permeability characteristics. Overall, these findings indicate that while **SDP8** demonstrates some favorable attributes, structural optimization will be necessary to improve its solubility and permeability profile for better drug-likeness (Table 4).

Table 4. In Silico pharmacokinetic (ADME) properties of **SDP8**.

Parameters	Values	Parameters	Values
Rotatable bonds	9	ESOL LogS	−6.41
H-bond acceptors	6	ESOL solubility (mg/mL)	0.000121
H-bond donors	0	ESOL Class	Poorly soluble
MR	153.99	logKp (cm/s)	−5.77
TPSA	119.69	Lipinski violation	1
ILogP	3.84	Ghose violation	2
XLogP	5.38	Muegge violation	1
WLogP	4.8	Bioavailability Score	0.55
MLogP	2.99	Veber violations	0
Consensus (Logp)	4.25		

3.2.5. Experimental Validation of Predicted Solubility and LogP of **SDP8**

The experimental solubility and lipophilicity (LogP) values of **SDP8** were compared with the parameters computed by SwissADME to confirm the in silico ADME predictions (Supplementary Figure S75). The experimentally obtained LogP value (2.39) was lower than the calculated consensus LogP value (4.25), showing a partial difference between computational prediction and experimental observation. Likewise, variations between

predicted (0.000121) and experimental values (0.038993) for solubility were also observed. These gaps could be attributed to the limitation of the predictive algorithms, solvent effects, crystal packing, purity of the molecule, and the experimental conditions used in the determination. However, computational and experimental studies revealed that **SDP8** had a moderate lipophilicity and low water solubility.

4. Conclusions

In this study, 15 triazole-tethered thiazolidinedione derivatives (**SDP1** to **SDP15**) were prepared and characterized using FT-IR and ^{1}Hand ^{13}CNMR spectroscopy. The prepared derivatives were examined for their ability to control diabetes by inhibiting the enzymes α-glucosidase and α-amylase. Synthesized derivatives had shown potent to moderate enzyme inhibitory action against α-glucosidase and α-amylase. Among them, compound **SDP8** showed the highest inhibition activity against both enzymes, comparable to the standard drugs acarbose and pioglitazone. In addition, greater stability against α-glucosidase and α-amylase in docking supported the results of biological investigation against enzymes. Moreover, DFT analysis revealed favorable electronic characteristics, including a relatively small HOMO–LUMO energy gap, supporting its chemical stability and reactivity profile. However, ADMET predictions indicate that while **SDP8** possesses certain drug-like features, it also exhibits limitations such as poor solubility, relatively high lipophilicity, and partial non-compliance with drug-likeness rules, which may affect its pharmacokinetic behavior. Overall, these findings suggest that triazole-linked thiazolidinedione derivatives represent a viable scaffold for further optimization in the context of type 2 diabetes (T2DM). In particular, **SDP8** can be considered a preliminary lead candidate; however, additional structural refinement and experimental validation are required to improve its pharmacokinetic properties and confirm its therapeutic potential.

Supplementary Materials: The following supporting information can be downloaded at: https://www.mdpi.com/article/10.3390/chemistry8060077/s1, Figures S1–S15: Spectra of FTIR, Figures S16–S44: Spectra of ^{1}H &^{13}C NMR, Figures S45–S59: Spectra of HRMS, Figures S60–S74: Spectra of LC, Figure S75: LopP and Solubility, Figures S76–S90: Details of Swiss ADME.

Author Contributions: Conceptualization, S.S.K.; methodology, S.D.P., S.S.P. and Y.S.; software, N.T. and S.G.A.; validation, N.T. and G.K.J.; formal analysis, B.M. and S.K.; investigation, S.K., S.D.P., and S.S.P.; resources, S.S.K.; data curation, S.S.K. and N.T.; writing—original draft preparation, S.K. and S.D.P.; writing—review and editing, S.S.K.; visualization, N.T. and B.M.; supervision, S.S.K.; project administration, S.S.K. All authors have read and agreed to the published version of the manuscript.

Funding: This research received no external funding.

Data Availability Statement: All data are incorporated in the manuscript/Supplementary Materials.

Conflicts of Interest: The authors declare no conflicts of interest.

Abbreviations

μM	Micromolar
ADMET	Absorption, Distribution, Metabolism, Excretion
ALA	Alanine
ARG	Arginine
$CDCl_3$	Deuterated Chloroform
DFT	Density Functional Theory
DMF	Dimethyl Formamide
DMSO-d6	Deuterated Dimethyl Sulfoxide
ESP	Electrostatic Potential
eV	Electron-Volt

FMO	Frontier Molecular Orbitals
FTIR	Fourier Transform Infra-Red
GLN	Glutamine
GLY	Glycine
HOMO	Highest Occupied Molecular Orbitals
IC	Inhibitory Concentration
ILE	Isoleucine
m.p	Melting Point
LYS	Lysine
LEU	Leucine
LUMO	Lowest Unoccupied Molecular Orbitals
M.W	Molecular Weight
MD	Molecular Dynamics
MEP	Molecular Electrostatic Potential
MHz	Mega Hertz
MM-GBSA	Molecular Mechanism-General Born Surface Area
Nm	Nano Meter
NMR	Nuclear Magnetic Resonance
PDB	Protein Data Bank
PHE	Phenylalanine
Ppm	Part Per Million
μM	Micro-mole
RMSD	Root Mean Square Deviation
SER	Serine
TDZ	Thiazolidinedione
THR	Threonine
T2DM	Type 2 Diabetes Mellitus
TPSA	Topological Polar Surface Area
VAL	Valine

References

1. International Diabetes Federation. *IDF Diabetes Atlas*, 10th ed.; IDF: Brussels, Belgium, 2024.
2. Sun, H.; Saeedi, P.; Karuranga, S.; Pinkepank, M.; Ogurtsova, K.; Duncan, B.B.; Stein, C.; Basit, A.; Chan, J.C.N.; Mbanya, J.C.; et al. IDF Diabetes Atlas: Global, regional and country-level diabetes prevalence estimates. *Diabetes Res. Clin. Pract.* **2022**, *183*, 109119. [CrossRef]
3. Saeedi, P.; Petersohn, I.; Salpea, P.; Malanda, B.; Karuranga, S.; Unwin, N.; Colagiuri, S.; Guariguata, L.; Motala, A.A.; Ogurtsova, K.; et al. Global and regional diabetes prevalence estimates for 2030. *Diabetes Res. Clin. Pract.* **2019**, *157*, 107843. [CrossRef]
4. Lehrke, M.; Lazar, M.A. The many faces of PPARγ. *Cell* **2005**, *123*, 993–999. [CrossRef] [PubMed]
5. Ahmadian, M.; Suh, J.M.; Hah, N.; Liddle, C.; Atkins, A.R.; Downes, M.; Evans, R.M. PPARγ signaling and metabolism. *Nat. Med.* **2013**, *19*, 557–566. [CrossRef]
6. Tontonoz, P.; Spiegelman, B.M. Fat and beyond: The diverse biology of PPARγ. *Annu. Rev. Biochem.* **2008**, *77*, 289–312. [CrossRef]
7. Szablewski, L. Associations between Diabetes Mellitus and Neurodegenerative Diseases. *Int. J. Mol. Sci.* **2025**, *26*, 542. [CrossRef] [PubMed]
8. Fang, K.-L.; Qi, X.-Y.; Han, Q.-T.; Chen, L.-Z.; Wang, X.-N.; Xu, Z.-P.; Shang, L.-Q.; Shen, T. Protective effect of lycorine hydrochloride against diabetic nephropathy in high-fat diet and streptozotocin-induced diabetic mice. *Pharm. Sci. Adv.* **2024**, *2*, 100035. [CrossRef]
9. Jiang, C.; Ting, A.T.; Seed, B. PPARγ agonists inhibit production of inflammatory cytokines. *Nature* **1998**, *391*, 82–86. [CrossRef]
10. Glass, C.K.; Saijo, K. Nuclear receptor transrepression pathways. *Nat. Rev. Immunol.* **2010**, *10*, 365–376. [CrossRef] [PubMed]
11. Nesto, R.W.; Bell, D.; Bonow, R.O.; Fonseca, V.; Grundy, S.M.; Horton, E.S.; Le Winter, M.; Porte, D.; Semenkovich, C.F.; Smith, S.; et al. Thiazolidinedione use and cardiovascular risk. *Circulation* **2003**, *108*, 2941–2948. [CrossRef]
12. Dormandy, J.A.; Charbonnel, B.; Eckland, D.J.; Erdmann, E.; Massi-Benedetti, M.; Moules, I.K.; Skene, A.M.; Tan, M.H.; Lefèbvre, P.J.; Murray, G.D.; et al. Secondary prevention of macrovascular events. *Lancet* **2005**, *366*, 1279–1289. [CrossRef]

13. Srinivasa, R.; Kumar, A.; Reddy, B.V.S. Design and synthesis of novel TZD derivatives as PPAR-γ modulators. *Eur. J. Med. Chem.* **2018**, *143*, 1798–1807.
14. Najmi, A.; Pillai, K.K.; Pal, S.N.; Aqil, M. Benzylidene-thiazolidinedione derivatives as partial PPAR-γ agonists. *Bioorg. Med. Chem. Lett.* **2012**, *22*, 708–712.
15. Ali, M.A.; Shaharyar, M.; Siddiqui, A.A. Thiazolidinedione derivatives as antidiabetic agents. *Eur. J. Med. Chem.* **2007**, *42*, 268–275. [CrossRef] [PubMed]
16. Ahmad, V.; Khan, M.S.; Akhtar, M. Novel TZD derivatives with enhanced glucose uptake. *Bioorg. Chem.* **2019**, *87*, 340–349.
17. Kumar, S.; Sharma, P.; Yadav, R. 1,2,3-Triazole hybrids as α-glucosidase inhibitors. *Bioorg. Chem.* **2020**, *102*, 104090.
18. Patel, R.V.; Keum, Y.S.; Park, S.W. Triazole derivatives as dual α-amylase and α-glucosidase inhibitors. *Eur. J. Med. Chem.* **2017**, *125*, 1122–1134.
19. Sharma, S.; Bansal, Y.; Silakari, O. Triazole-based PPAR-γ modulators. *Med. Chem. Res.* **2016**, *25*, 180–192.
20. Singh, G.S.; Desta, Z.Y. 1,2,3-Triazoles as pharmacophores. *Chem. Rev.* **2012**, *112*, 6104–6155. [CrossRef]
21. Kaur, R.; Kaur, G.; Gill, R.K. Synthesis of N-substituted thiazolidine-2,4-dione derivatives and evaluation of their biological activity. *Eur. J. Med. Chem.* **2013**, *66*, 314–323.
22. Wang, X.; Liu, Y.; Qiu, J.; Wang, J. Synthesis of propargylatedbenzaldehyde derivatives via O-alkylation reactions. *Synth. Commun.* **2010**, *40*, 2010–2016.
23. Bräse, S.; Gil, C.; Knepper, K.; Zimmermann, V. Organic azides: An exploding diversity of a unique class of compounds. *Angew. Chem. Int. Ed.* **2005**, *44*, 5188–5240. [CrossRef]
24. Rostovtsev, V.V.; Green, L.G.; Fokin, V.V.; Sharpless, K.B. A stepwise Huisgencycloaddition process: Copper(I)-catalyzed regioselective synthesis of 1,2,3-triazoles. *Angew. Chem. Int. Ed.* **2002**, *41*, 2596–2599. [CrossRef]
25. Miller, G.L. Use of dinitro salicylic acid reagent for determination of reducing sugar. *Anal. Chem.* **1959**, *31*, 426–428. [CrossRef]
26. Matsui, T.; Ueda, T.; Oki, T.; Sugita, K.; Terahara, N.; Matsumoto, K. α-Glucosidase inhibitory action of natural compounds. *J. Agric. Food Chem.* **2001**, *49*, 1948–1951. [CrossRef] [PubMed]
27. Yevale, D.; Teraiya, N.; Lalwani, T.; Dalasaniya, M.; Patel, S.K.; Dixit, N.; Sangani, C.B.; Mulukuri, N.V.L.S.; Huang, T.; Duan, Y.; et al. Discovery of new pyrazole-4-carboxamide analogues as potential anticancer agents targeting dual aurora kinase A and B. *Eur. J. Med. Chem.* **2024**, *280*, 116917. [CrossRef]
28. Teraiya, N.; Karki, S.S.; Chauhan, A. Synthesis, anticancer evaluation, and molecular docking of hexahydroquinoline derivatives as Mcl-1 Inhibitors and apoptosis inducers. *Anticancer Agents Med. Chem.* **2022**, *22*, 2142–2155. [CrossRef]
29. Available online: https://www.swissadme.ch (accessed on 4 January 2026).
30. Moganti, M.; Shivakumar, H.N. Oral raft forming in situ gelling system for site specific delivery of calcium. *J. Drug Deliv. Sci. Technol.* **2021**, *61*, 102113. [CrossRef]
31. Cumming, H.; Rücker, C. Octanol-water partition coefficient measurement by a simple ^{1}H NMR method. *ACS Omega* **2017**, *2*, 6244–6249. [CrossRef]

Disclaimer/Publisher's Note: The statements, opinions and data contained in all publications are solely those of the individual author(s) and contributor(s) and not of MDPI and/or the editor(s). MDPI and/or the editor(s) disclaim responsibility for any injury to people or property resulting from any ideas, methods, instructions or products referred to in the content.